Three-dimensional initial data for the collision of two black holes. II. Quasicircular orbits for equal-mass black holes

Gregory B. Cook
Center for Radiophysics and Space Research, Cornell University, Ithaca, New York 14853
(Received 25 April 1994)

The construction of initial-data sets representing binary black-hole configurations in quasicircular orbits is studied in the context of the conformal-imaging formalism. An effective-potential approach for locating quasicircular orbits is outlined for the general case of two holes of arbitrary size and with arbitrary spins. Such orbits are explicitly determined for the case of two equal-sized nonrotating holes, and the innermost stable quasicircular orbit is located. The characteristics of this innermost orbit are compared to previous estimates for it, and the entire sequence of quasicircular orbits is compared to results from the post-Newtonian approximation. Some aspects of the numerical evolution of such data sets are explored.

PACS number(s): 04.25.Dm, 04.70.Bw, 97.80.Fk

I. INTRODUCTION

The numerical simulation of binary black-hole systems begins with the specification of appropriate initial data. A general method for specifying the initial data of binary black-hole systems has been described in Cook *et al.* [1] (hereafter paper I). Because of the circularizing effects of gravitational radiation damping, we expect the orbits of most tight binary systems to have small eccentricities. Therefore, a method is needed which can discern which data sets, within the very large parameter space of binary black-hole initial-data sets, correspond to binary black holes in a quasicircular orbit. In this paper, I will describe such a method and explicitly compute the initial-data parameters necessary for describing the quasicircular orbit of two equal-sized nonrotating black holes. In addition, this method yields an estimate of the innermost stable quasicircular orbit for two equal-sized black holes.

The general framework being used for defining initial-data sets containing black holes is known as the *conformal-imaging formalism* [2–7]. It is based on the Arnowitt-Deser-Misner (ADM) [8], or 3+1, decomposition of Einstein's equations, York's conformal and transverse-traceless decompositions of the constraint equations, and a method of imaging applicable to tensors. Application of this approach to the case of two black holes with arbitrary linear and angular momenta on each hole has been explored in paper I. In that work, three independent numerical approaches were described for constructing initial-data sets. I will make use, in this paper, of the "Čadež-coordinate approach" for solving the Hamiltonian constraint, a three-dimensional (3D) quasilinear elliptic partial differential equation.

Using numerical initial-data sets, an "effective potential" can be constructed which consists of the gravitational binding energy between the holes plus the kinetic energy of the holes, with the restriction that all physical parameters characterizing the system are held fixed except for the separation of the holes. If we fix the momenta of the holes appropriately, then an initial-data set occurring at a minimum of the effective potential will represent two black holes in a quasicircular orbit. For the case of two equal-sized holes with no intrinsic rotation, the set of physical parameters that must be held fixed contains only the orbital angular momentum of the system. For this simple case, we have located those initial-data sets which represent two black holes in quasicircular orbit at various separations. As expected [9,10], there is some minimum separation required before a minimum of the effective potential exists. This minimum separation serves as an estimate for the point at which the secular inspiral of the two holes ends and the final dynamical plunge to coalescence occurs.

I will begin with a description of the parameter space of 3D initial-data sets, a brief description of how initial-data sets are constructed, and how the physical parameters associated with a given data set are computed. I will continue with a description of the effective-potential method as applied to initial data constructed via the conformal-imaging approach. Using this method, I explicitly locate the sequence of quasicircular orbits (as a function of separation) for equal-sized holes and compare this sequence to the results obtained via a post-Newtonian analysis. Also, the characteristics of the innermost stable quasicircular orbit are compared to the results of previous estimates for this orbit. I conclude with some observations about the eventual evolution of initial-data sets representing two equal-sized holes in quasicircular orbits.

II. INITIAL DATA

A detailed description of how binary black-hole initial-data sets are constructed within the conformal-imaging formalism is given in paper I and references therein. In brief, the configuration is parametrized first by fixing the locations $\mathbf{C}_1$ and $\mathbf{C}_2$ of the two holes in a Cartesian flat conformal *background* space along with the radii a_1 and a_2 of the two holes. If we let a_1 set the fundamental length scale of the problem, then we can parametrize

the physical locations and relative sizes of the holes in the background space by two dimensionless parameters α and β defined by

$$\alpha \equiv \frac{a_1}{a_2} \tag{1}$$

$$\beta \equiv \frac{|\mathbf{C}_1 - \mathbf{C}_2|}{a_1}. \tag{2}$$

In addition to the locations and sizes of the holes, we also specify for each hole both a linear momentum vector $\mathbf{P}_{1,2}$ and an angular momentum vector $\mathbf{S}_{1,2}$. The physical meaning of these momenta is seen in the following way. For a single isolated hole, the *physical* linear and angular momenta contained in the initial-data set, as measured at infinity, are given directly by the parameters $\mathbf{P}$ and $\mathbf{S}$. For two holes, the total physical linear momentum of the system is simply the vector sum $\mathbf{P}_1 + \mathbf{P}_2$. The total physical angular momentum is given by the vector sum $\mathbf{S}_1 + \mathbf{S}_2 + \mathbf{J}$, where $\mathbf{J}$ is the orbital angular momentum of the system which will be described in detail below. With a_1 setting the fundamental length scale, we find that the momenta of two black holes within the initial-data set is completely specified by the four dimensionless vector parameters: $\mathbf{P}_1/a_1$, $\mathbf{P}_2/a_1$, $\mathbf{S}_1/a_1^2$, and $\mathbf{S}_2/a_1^2$.

Aside from the complications of a given numerical technique used to solve for the initial data, we see that the specification of a general two-hole configuration requires that fourteen dimensionless parameters be fixed. Having chosen these fourteen parameters, an initial-data set is constructed by solving the momentum and Hamiltonian constraints of general relativity as outlined in paper I. The particular numerical technique used to solve the Hamiltonian constraint in this work is the "Čadež-coordinate approach" described in detail in Sec. III A of that paper and references therein.

Once the initial-data set has been computed, various physical parameters characterizing the data set can be computed. In particular, the following quantities are calculated: the ADM energy of the system E, the proper surface areas of the marginally outer-trapped surfaces defining each individual hole $A_{1,2}$, the dipole moment of the energy distribution $\mathbf{d}$, and the shortest proper separation between the two marginally outer-trapped surfaces ℓ. Definitions for the ADM energy and the dipole moment can be found in Eqs. (24) and (25) of Ref. [7]. Note that it is actually the dimensionless ratios E/a_1, $A_{1,2}/a_1^2$, $\mathbf{d}/a_1^2$, and ℓ/a_1 which are computed. These quantities, together with the initial-data parameters, allow us to compute the orbital angular momentum $\mathbf{J}$ of the system. Generalizing the calculation found in Ref. [11], it is straightforward to show that the orbital angular momentum for a configuration of two black holes is given by

$$\mathbf{J} = (\mathbf{C}_1 - \mathbf{O}) \times \mathbf{P}_1 + (\mathbf{C}_2 - \mathbf{O}) \times \mathbf{P}_2, \tag{3}$$

where $\mathbf{O}$ is the point in the background space about which the angular momentum is defined. The only unique choice for $\mathbf{O}$ is the center of energy of the system which, if chosen as the origin of coordinates, results in a vanishing dipole moment. Using the definition of the ADM energy and the dipole moment, it follows that the center of energy is at $\mathbf{O} = \mathbf{d}/E$. Therefore, the general definition of the orbital angular momentum is

$$\mathbf{J} \equiv \left(\mathbf{C}_1 - \frac{\mathbf{d}}{E}\right) \times \mathbf{P}_1 + \left(\mathbf{C}_2 - \frac{\mathbf{d}}{E}\right) \times \mathbf{P}_2. \tag{4}$$

III. THE EFFECTIVE-POTENTIAL METHOD

The definitions of the ADM energy, total linear and angular momenta at infinity, the dipole moment, the proper separation of the holes, and the areas of the two marginally outer-trapped surfaces are rigorously defined physical quantities. To define the effective potential of a configuration, it is necessary to use the concepts of the masses and spins of the individual black holes and to have a measure of the effective binding energy between the two holes. However, none of these quantities are rigorously defined in general relativity for a strong-field nonstationary configuration.

In the limit of large separations and small linear momenta and spin on the holes, the following definitions hold. The mass of each hole can be defined via the Christodoulou formula [12]

$$M^2 = M_{\rm ir}^2 + \frac{S^2}{4M_{\rm ir}^2}, \tag{5}$$

with the irreducible mass $M_{\rm ir} \approx \sqrt{A/16\pi}$ and S being the magnitude of the spin on the hole. As shown in the Appendix, we can approximate S for each hole by the magnitude of its respective spin parameter $|\mathbf{S}_{1,2}|$. Though it seems possible that the linear momentum on one hole could *induce* a spin on the other hole, this is, in fact, not the case. Thus, the quantity $\mathbf{J}$, which we identified above as the orbital angular momentum, is not contaminated by an induced spin on the holes. We are therefore justified in defining the orbital angular momentum of the system by Eq. (4), and we define the spins of the individual holes via their respective spin parameters. Finally, the effective binding energy E_b between the holes is defined as

$$E_b \equiv E - M_1 - M_2, \tag{6}$$

where $M_{1,2}$ are the masses of the two holes as defined above. Note that the effective binding energy contains both the gravitational binding energy between the two holes and their orbital kinetic energies, but not the rotational kinetic energy of the individual holes.

These definitions are rigorous only in the limit of infinite separation and zero momenta on either hole. The limit of zero momenta on the holes is required because initial-data sets containing a single black hole constructed via the conformal-imaging approach necessarily contain some spurious gravitational wave energy [13]. The same is true of multihole initial-data sets, however, Cook and Abrahams [14] have shown that the spurious radiation content for the case of two holes is quite small

so long as the holes are modestly separated and the momenta are not excessively large. We will find that these constraints are satisfied for the majority of configurations of physical interest.

Henceforth, we will take the masses of the holes, their spins, mutual binding energy, and orbital angular momentum to be *defined* as given above.

We turn now to the definition of an effective potential useful for determining the location of quasicircular orbits. In general, such an effective potential should be a function of the separation and sizes of the holes, the orbital angular momentum of the system, the spins of the holes, and the gravitational radiation content of the system. Within the conformal-imaging approach, one has no freedom in specifying the radiation content of the system. This is fixed by the demands that the spatial three-metric be conformally flat and that all fields satisfy an isometry condition (cf. Ref. [7]). With this restriction, we see that the effective potential should be a function of *nine* physical parameters but a general two-hole initial-data set depends on fourteen initial-data parameters.

To reduce the size of this parameter space, we first demand that the configuration be in a center of momentum frame. This restriction requires

$$\mathbf{P}_1 + \mathbf{P}_2 = 0. \tag{7}$$

A configuration representing a quasicircular orbit should satisfy

$$\mathbf{P}_{1,2} \cdot (\mathbf{C}_2 - \mathbf{C}_1) = 0. \tag{8}$$

Together, Eqs. (7) and (8) reduce the fourteen-dimensional initial-data parameter space to nine dimensions. These parameters are α, β, the magnitude of the linear momentum on either hole P/a_1, $\mathbf{S}_1/a_1^2$, and $\mathbf{S}_2/a_1^2$.

The respective dimensionless physical parameters of the effective potential are $X \equiv M_1/M_2$, ℓ/m, $J/\mu m$, $\mathbf{S}_1/M_1^2$, and $\mathbf{S}_2/M_2^2$ where $M_{1,2}$ are the masses of the individual holes, $m \equiv M_1 + M_2$ is the total mass, $\mu \equiv M_1 M_2/m$ is the reduced mass, and J is the magnitude of the orbital angular momentum of the system. Finally, the dimensionless effective potential is given by the binding energy as E_b/μ.

Finding quasicircular orbits is now a conceptually easy task. We compute E_b/μ as a function of ℓ/m while holding the remaining eight *physical* parameters constant. A minimum in E_b/μ then corresponds to a "stable" quasicircular orbit. In addition to locating the quasicircular orbits, we can also estimate the orbital angular velocity Ω of the system as measured at infinity. This is given by taking the derivative of the binding energy with respect to the orbital angular momentum while holding all other parameters fixed. In dimensionless form then one obtains

$$m\Omega = \frac{\partial E_b/\mu}{\partial J/\mu m}. \tag{9}$$

Though conceptually straightforward, the computational task of locating quasicircular orbits is difficult. The main difficulty arises from the fact that the physical parameters that must be held fixed are not independently correlated with their respective initial-data parameters. That is, holding eight of the nine initial-data parameters fixed while varying β will not result in an effective-potential curve. We see then that, in general, the problem of determining *one* quasicircular orbit is quite involved. It requires finding the roots of eight functions, each of which depends on eight parameters, at each value of the separation at which the effective potential is evaluated.

Fortunately, the size of this parameter space can be cut in half. The only definition we have available for the direction of the spins of the holes (see the Appendix) is the direction of their respective initial-data spin parameters. The directions of the spins are then fixed relative to the separation of the holes and the plane of the orbit, which are defined by $\mathbf{P}_{1,2}$ and $\mathbf{C}_2 - \mathbf{C}_1$. This direction is independent of the numerical solution of the Hamiltonian constraint, so only the magnitude of the two initial-data spin-vector parameters needs to be varied to hold the physical parameters fixed. As a result, for a fixed value of β the following four equations must be satisfied:

$$X_{(\alpha,P/a_1,S_1/a_1^2,S_2/a_1^2;\beta)} = X_0 \tag{10a}$$

$$\left[\frac{J}{\mu m}\right]_{(\alpha,P/a_1,S_1/a_1^2,S_2/a_1^2;\beta)} = \left.\frac{J}{\mu m}\right|_0 \tag{10b}$$

$$\left[\frac{S_1}{M_1^2}\right]_{(\alpha,P/a_1,S_1/a_1^2,S_2/a_1^2;\beta)} = \left.\frac{S_1}{M_1^2}\right|_0 \tag{10c}$$

$$\left[\frac{S_2}{M_2^2}\right]_{(\alpha,P/a_1,S_1/a_1^2,S_2/a_1^2;\beta)} = \left.\frac{S_2}{M_2^2}\right|_0. \tag{10d}$$

When these four equations are satisfied, Eq. (6) yields a value of the effective potential E_b/μ at some value of the physical separation ℓ/m. Changing the value of β and resolving Eqs. (10a)–(10d) results in another value of the effective potential at a different separation.

IV. EQUAL-MASS NONROTATING HOLES

The simplest application of the effective-potential method is to the case of two equal-sized black holes with no intrinsic spin. In this problem, $S_1/a_1^2 = S_2/a_1^2 = 0$ and, because of the symmetry between the holes, we know that $\alpha = 1 \rightarrow X = 1$. Therefore, solving for the effective potential requires solving only Eq. (10b) as a function of P/a_1 alone for a given β.

The method used to solve Eq. (10b) is the following. For a given value of β, the initial-value equations are solved at a sufficiently large number of values of P/a_1 in order to encompass all of the values of $J/\mu m$ at which we want to evaluate the effective potential. Using interpolation, we can estimate new values of P/a_1 that will yield solutions near the desired values of $J/\mu m$; the procedure is repeated until any errors introduced by interpolation

are sufficiently small. The most difficult part of the problem is to solve the initial-value equations with sufficient accuracy. Typically, both the ADM mass E/a_1 and the areas of the marginally outer-trapped surfaces $A_{1,2}/a_1^2$ need to be determined to a relative error of $\sim 10^{-5}$.

Currently, the only numerical method capable of solving the initial-value equations to this accuracy is the multigrid-based Čadež-coordinate approach described in detail in Sec. III A of paper I. Such high accuracy can be obtained through the use of Richardson extrapolation. As described in paper I, the Čadež-coordinate approach used to solve the Hamiltonian constraint results in a numerical solution for the conformal factor $\psi^{\rm num}$, which has an asymptotic ($h \to 0$) expansion given by

$$\psi^{\rm num} = \psi + h^2 e_2^{\psi} + h^4 e_4^{\psi} + \cdots, \tag{11}$$

where ψ is the analytic solution of the Hamiltonian constraint, h is the basic scale of discretization, and $e_2^{\psi}, e_4^{\psi}, \ldots$ are h-independent functions. In addition, the numerical integrals for E/a_1, $\mathbf{d}/a_1^2$, $A_{1,2}/a_1^2$, and ℓ/a_1 have all been constructed to yield analogous error expansions that depend strictly on powers of h^2.

One final source of error which must be examined comes from the necessity of imposing an approximate outer-boundary condition (cf. Ref. [7]). In order to minimize the effects of this approximation, the outer boundary has been placed at a distance of at least $2000a_1$ from the holes.

Figure 1 displays a set of effective-potential curves for a wide range of values for $J/\mu m$. The displayed curves are interpolated results derived from 3000 Richardson-extrapolated data points, each resulting from the extrapolation of three separate solutions of the initial-value equations at resolutions similar to those described in paper I. All solutions were generated on an IBM-SP1 parallel computer and required a total computational time in excess of 3000 CPU hours. The value of $J/\mu m$ is held fixed along each of the thin curves which plots the effective potential E_b/μ as a function of the proper separation of the holes ℓ/m. The bold curve crossing several of the effective-potential curves represents a sequence of quasicircular orbits. This can be seen more clearly in Fig. 2 where the region containing minima in the effective-potential curves is shown in expanded form. The bold line representing the sequence of quasicircular orbits begins at the right at an $\ell/m \sim 14$. This line should, of course, extend to larger values of ℓ/m, but data has not been computed in this regime. Following the sequence of quasicircular orbits to smaller values of ℓ/m, we find that the minimum in the effective potential vanishes. At this point, the sequence of quasicircular orbits terminates at an innermost stable orbit.

For $\ell/m \lesssim 4$ we notice that some of the effective-potential curves pass through a local maximum and a second minimum. These additional minima should not be interpreted as a new sequence of stable quasicircular orbits. Rather, this behavior indicates that the approximations outlined in Sec. III, especially the identification of Eq. (6) as a measure of the binding energy between the holes, are breaking down. This assertion is justified on the following grounds. Anninos *et al.* [15] have shown that for time-symmetric initial data constructed via the conformal-imaging approach an *event horizon* en-

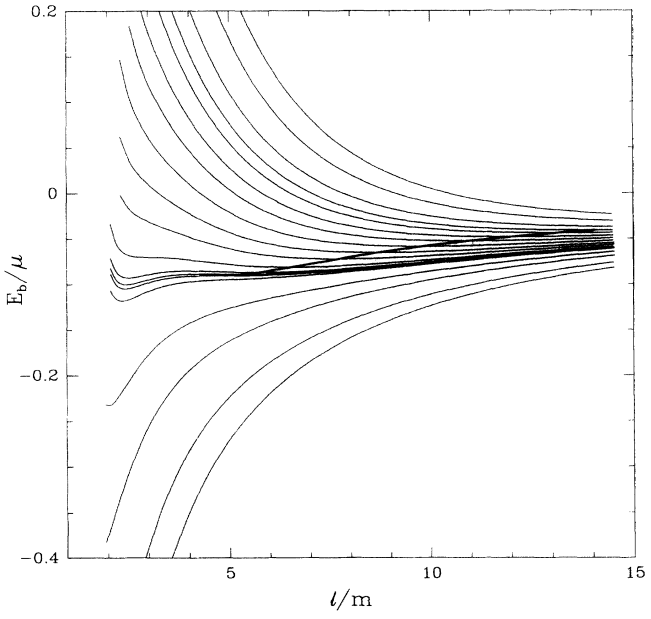

FIG. 1. The effective potential E_b/μ as a function of separation ℓ/m for the following values of the orbital angular momentum $J/\mu m$: 1.5, 2, 2.5, 2.75, 2.95, 2.976, 2.985, 3, 3.05, 3.15, 3.25, 3.37, 3.5, 3.62, 3.75, 3.85, 4, 4.25, and 4.5. These values of $J/\mu m$ label, respectively, curves from the bottom of the figure to the top. Also, plotted as a bold line is the sequence of quasicircular orbits which cross the effective-potential curves at local minima.

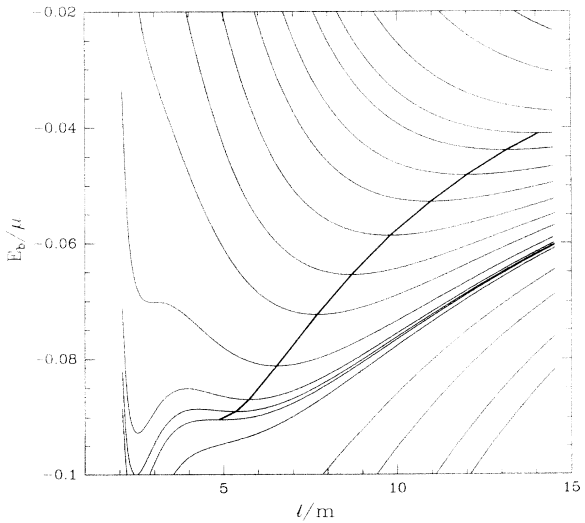

FIG. 2. An enlargement of the section of Fig. 1 which contains the sequence of quasicircular orbits. This sequence begins at the innermost stable quasicircular orbit near $\ell/m = 5$ on the $J/\mu m = 2.976$ curve and extends in the direction of larger separation. In the figure, the sequence terminates at the minimum of the $J/\mu m = 3.85$ effective-potential curve, although it should continue.

compasses both holes on the initial-data slice when their separation parameter μ (not to be confused with the reduced mass) is less than about 1.8. This corresponds to a separation parameter of $\beta \sim 6.2$ and to a proper separation of $\ell/m \sim 3$. For the case of orbiting holes, we expect the effects of angular momentum to delay the onset of formation of a common event horizon based on both physical intuition and the axisymmetric results of Cook and Abrahams [14]. Thus, we should expect a common event horizon for $\ell/m < 3$ and, further, that the effective-potential method being used should not be trusted for $\ell/m < 4$.

The characteristics of initial-data sets representing quasicircular orbits of two equal-sized, nonrotating black holes are given in Table I. In addition to the physical parameters characterizing the system (ℓ/m, E_b/μ, $J/\mu m$, and $m\Omega$), the table contains the initial-data parameters P/a_1 and β required to reproduce these particular data sets. Note that all initial-data sets described in this paper satisfy the *minus* isometry condition of the conformal-imaging approach. Values in this table should be considered accurate to better than 1% with the exception of $m\Omega$, which should be considered accurate to a few percent.

In order to gauge the accuracy with which we have located the innermost stable quasicircular orbit, note that in the limit of a test mass orbiting a Schwarzschild black hole, the proper separation between the event horizon and the test mass is found to be

$$\frac{\ell}{m} = 2\ln\left(\frac{1+\sqrt{2/3}}{1-\sqrt{2/3}}\right) \approx 4.58. \tag{12}$$

This should be compared with a value of $\ell/m = 4.88$ obtained from Table I. The ratio of these two values is 0.94. Kidder *et al.* [10] obtain an analogous ratio of 0.96, where separation is measured in terms of harmonic or de Donder coordinates. Kidder *et al.* obtain this result via a critical point analysis of the equations of motion through (post)^2-Newtonian order. After altering the equations of motion significantly to reproduce exactly the test mass limit, Kidder *et al.* find that the ratio has changed to 0.83 and that the innermost stable circular orbit is characterized by the following physical parameters: $E_b/\mu \sim -0.0378$, $J/\mu m \sim 3.83$, and $m\Omega \sim 0.0605$. A comparison of these values with Table I shows that Kidder *et al.* are finding an innermost stable circular orbit in which the holes are much farther apart than we find with the effective-potential method. In contrast with this, Blackburn and Detweiler [9] have used a variational principle together with the assumption of a periodic solution to Einstein's equations to obtain an estimate for the innermost orbit for two equal-sized holes. Using a single trial geometry, which they call "rather unsophisticated," they obtain an innermost orbit characterized by $E_b/\mu \sim -0.65$, $J/\mu m \sim 0.85$, and $m\Omega \sim 2$. Such an orbit is much more tightly bound than seems possible from the effective-potential method. Blackburn and Detweiler point out that the assumptions of their variational principle have been violated by the time this innermost circular orbit is reached. However, they describe a less tightly bound circular orbit that should not be in violation of the underlying assumptions of their approach. This orbit has a binding energy of $E_b/\mu \sim -0.28$, which is still three times larger than the binding energy obtained in this paper for the innermost stable quasicircular orbit.

TABLE I. Physical and initial-data parameters characterizing certain configurations along the sequence of stable quasicircular orbits. The data sets represented in this table have been constructed using the *minus* isometry condition of the conformal-imaging approach.

ℓ/m	E_b/μ	$J/\mu m$	$m\Omega$	P/a_1	β
4.880	−0.090 30	2.976	0.172	1.685	11.82
5.365	−0.088 90	2.985	0.145	1.392	13.28
5.735	−0.086 84	3.000	0.130	1.230	14.43
6.535	−0.081 12	3.050	0.104	0.9868	16.99
7.700	−0.072 26	3.150	0.0774	0.7752	20.84
8.695	−0.065 34	3.250	0.0622	0.6613	24.21
9.800	−0.058 62	3.370	0.0504	0.5734	28.04
10.96	−0.052 70	3.500	0.0414	0.5066	32.15
12.02	−0.048 10	3.620	0.0352	0.4609	35.93
13.16	−0.043 88	3.750	0.0300	0.4218	40.06
14.07	−0.041 04	3.850	0.0270	0.3960	43.38

V. THE POST-NEWTONIAN LIMIT

Comparison with previous estimates for the innermost stable quasicircular orbit of two equal-mass nonrotating black holes is far from yielding a consensus as to its proper value. However, we can gain some insight into the reliability of the results derived in this paper by comparing the sequence of quasicircular orbits against the post-Newtonian description of circular orbits. Based on the (post)^2-Newtonian results of Kidder *et al.* [16] for the binding energy, angular momentum, and equations of motion for a binary system with a circular orbit, it is straightforward to show that the binding energy and angular momentum of two compact objects in a circular orbit must satisfy

$$\frac{E_b}{\mu} = -\frac{1}{2}\left(\frac{\mu m}{J}\right)^2\left[1+\frac{1}{4}(9+\eta)\left(\frac{\mu m}{J}\right)^2+\left(\frac{81}{8}-\frac{7}{8}\eta+\frac{1}{8}\eta^2\right)\left(\frac{\mu m}{J}\right)^4+\cdots\right] \tag{13}$$

$$\frac{E_b}{\mu} = -\frac{1}{2}(m\Omega)^{2/3}\left[1-\frac{1}{12}(9+\eta)(m\Omega)^{2/3}-\left(\frac{27}{8}-\frac{19}{8}\eta+\frac{1}{24}\eta^2\right)(m\Omega)^{4/3}+\cdots\right] \tag{14}$$

$$\left(\frac{J}{\mu m}\right)^2 = (m\Omega)^{-2/3}\left[1+\frac{1}{3}(9+\eta)\,(m\Omega)^{2/3}+\left(9-\frac{17}{4}\eta+\frac{1}{9}\eta^2\right)(m\Omega)^{4/3}+\cdots\right], \tag{15}$$

where $\eta \equiv \mu/m$. The three terms inside the square brackets represent the Newtonian results for circular orbits along with the first and second post-Newtonian corrections.

Figure 3 compares the numerical results for binding energy versus orbital angular momentum for the sequence of quasicircular orbits against Eq. (13) with $\eta = 1/4$. The numerical data are displayed as a bold solid line with cross marks denoting actual data points. The long dashed line corresponds to the Newtonian result, the short dashed line to the Newtonian result together with the (post)^1-Newtonian corrections, and the dotted line to the full (post)^2-Newtonian result. Notice that for large $J/\mu m$ (large separation), the post-Newtonian expansion appears to be converging quite well toward the numerical result. Figures 4 and 5 are analogous plots for the orbital angular momentum versus orbital angular frequency and binding energy versus orbital angular frequency, respectively. Again, in the limit of large separation (small $m\Omega$), the post-Newtonian expansions appear to converge well with the numerical results. This agreement at large separations, together with the general agreement in the shapes of the curves when the separation decreases, confirms that the basic premises adopted in the definition of the effective-potential method are sound. For small separations, we know that the approximations needed to define the effective potential as outlined in Sec. III must be questioned. Unfortunately, the post-Newtonian approximation also breaks down as the separation of the holes becomes small and, it is impossible to gauge the validity of the approximations based on the post-Newtonian results.

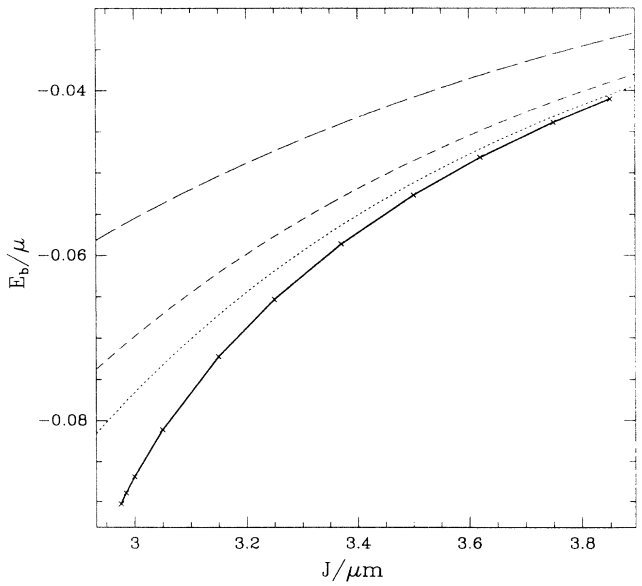

FIG. 3. The effective potential E_b/μ as a function of the orbital angular momentum $J/\mu m$ for quasicircular orbits. The solid line corresponds to the sequence of quasicircular orbits computed in this paper. The long dashed line is the result obtained from Newtonian theory. The short dashed line is the result based on (post)^1-Newtonian theory, and the dotted line is the result based on (post)^2-Newtonian theory.

VI. DISCUSSION

The most important use of the results obtained in this paper is to narrow the range of initial-data parameters which must be considered in setting up an actual numerical simulation of the inspiral and collision of two black holes. Assuming one is interested in evolving initial data that represents something similar to a quasicircular orbit, then the results presented in Table I allow us to estimate the minimum length of time that the system must be evolved, as well as some limits on the final state of the system.

Beginning with the latter, let us assume that the binary system coalesces and settles down to a Kerr hole with mass M_f and angular momentum J_f. From Eq. (5) we know that the Kerr ratio J_f/M_f^2 is

$$\frac{J_f}{M_f^2} = \frac{J_f/M_{\rm ir}^2}{1+\frac{1}{4}\left(J_f/M_{\rm ir}^2\right)^2}, \tag{16}$$

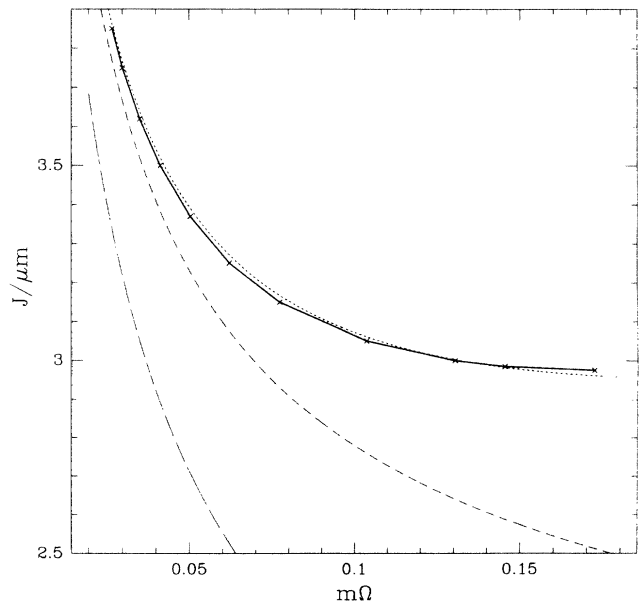

FIG. 4. The orbital angular momentum $J/\mu m$ as a function of the orbital angular velocity $m\Omega$. Lines are as indicated in Fig. 3.

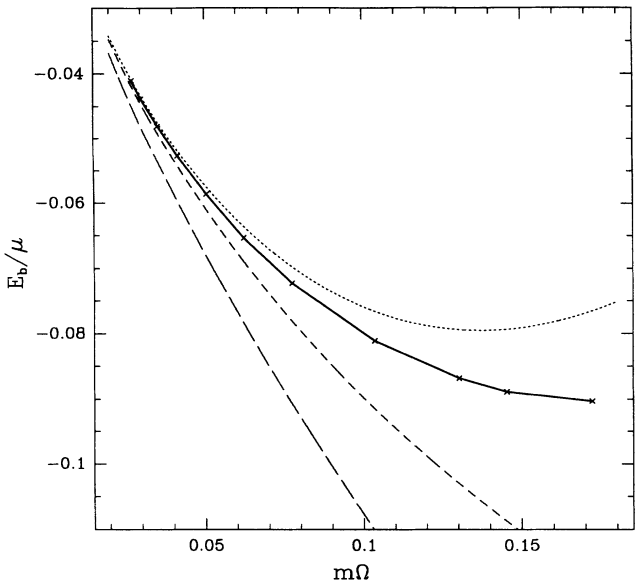

FIG. 5. The effective potential E_b/μ as a function of the orbital angular velocity $m\Omega$. Lines are as indicated in Fig. 3.

where we now let $M_{\rm ir}$ denote the irreducible mass of the final Kerr hole. Assuming only that the individual holes do not rotate, we know that the irreducible mass is bounded by

$$M_{\rm ir} \geq \sqrt{M_1^2 + M_2^2} = m\sqrt{1-2\eta}, \tag{17}$$

where M_1, M_2, etc. are defined as before. Since we know that $J_f \leq J$, we find that

$$\frac{J_f}{M_{\rm ir}^2} \leq \frac{\eta}{1-2\eta}\frac{J}{\mu m}. \tag{18}$$

Examining Eqs. (16) and (18) we find that, so long as $J_f/M_{\rm ir}^2 < 2$, the Kerr ratio J_f/M_f^2 is *guaranteed* to be less than unity. For equal-sized holes, this implies that the Kerr ratio is satisfied as long as $J/\mu m < 4$. If we evolve initial data representing the innermost stable quasicircular orbit, we find that $J_f/M_f^2 \leq 0.958$. If we make the severe assumptions that all of the binding energy "released" in the coalescence is recaptured by the resulting black hole and that half of the angular momentum is, nevertheless, radiated away during the final plunge and coalescence, we find that $J_f/M_f^2 \sim 0.4$. We see then that a black hole resulting from the inspiral and final plunge of two nonrotating black holes must certainly be considered to be rapidly rotating, but it will not violate the Kerr limit.

Now consider the minimal requirements of a numerical evolution of binary coalescence in the case of two equal-sized, nonrotating black holes. If the simulation is to remotely resemble the final plunge of two holes following a secular inspiral, then our best guess at initial data is that for the innermost stable quasicircular orbit. From the estimate of the orbital angular velocity in Table I, we find that the orbital period is $\tau \sim 37m$. It is reasonable to assume that the final plunge will occur on a time scale comparable to that of the innermost orbit. If this initial data leads to an evolution that begins at the most one orbit before the beginning of the final plunge and we add to the evolution time a period sufficient to watch some of the ring-down, then we find that the numerical simulation must be capable of evolving for 90–130m.

ACKNOWLEDGMENTS

I gratefully acknowledge many useful discussions with Andrew Abrahams, Stuart Shapiro, and Saul Teukolsky. Special thanks go to Curt Cutler and Lawrence Kidder for helpful discussions and for contributions to the post-Newtonian comparison. This work was supported in part by National Science Foundation Grant No. PHY 90-07834. Computations were performed at the Cornell Center for Theory and Simulation in Science and Engineering, which was supported in part by the National Science Foundation, IBM Corporation, New York State, and the Cornell Research Institute.

APPENDIX: THE MOMENTA OF INDIVIDUAL HOLES

A rigorous quasilocal definition of momentum requires the presence of a Killing vector field $\xi^i_{(k)}$. The magnitude of the momentum associated with $\xi^i_{(k)}$ within a given surface contained in a spatial slice is denoted $\Pi_{(k)}$, where

$$\Pi_{(k)} \equiv \Pi_i \xi^i_{(k)} = \frac{1}{8\pi}\oint \left(K^j_i - \delta^j_i K\right)\xi^i_{(k)} d^2 S_j. \tag{A1}$$

Here, K^i_j is the extrinsic curvature of the slice and K is its trace. A general spatial slice contains no Killing vectors and only the total momenta of an asymptotically flat spatial slice can be defined. This definition requires integrating Eq. (A1) at spatial infinity using *asymptotic* Killing vectors $\bar{\xi}^i_{(k)}$, which are Killing vectors of the flat metric to which the physical metric is asymptotic. Note, however, that the *angular* momentum will only be gauge-invariant if $\bar{\xi}^i_{(k)}$ is an exact symmetry of the physical metric (cf. York [17]).

Now consider the momenta of gravitational initial data constructed within the conformal-imaging approach. Following this approach, we conformally decompose the physical metric of a spatial slice as $\gamma_{ij} = \psi^4 \bar{\gamma}_{ij}$, where $\bar{\gamma}_{ij}$ is the *flat* conformal background metric and ψ is the conformal factor. With the trace-free conformal background extrinsic curvature, defined by $\bar{A}^i_j = \psi^6(K^i_j - \frac{1}{3}\delta^i_j K)$ and with $K = 0$, we can rewrite equation (A1) as

$$\Pi_{(k)} = \frac{1}{8\pi}\oint_\infty \bar{A}^j_i \bar{\xi}^i_{(k)} d^2 \bar{S}_j. \tag{A2}$$

This form of the equation has the advantage that it does not involve the conformal factor ψ, so we can compute the momentum without having a solution of the Hamiltonian constraint. Also, I emphasize that we have *not* used the

fact that $\psi \to 1$ at spatial infinity in deriving Eq. (A2), so that if $\bar{\xi}^i_{(k)}$ represents an exact symmetry of the *physical* metric, then Eq. (A2) can be evaluated (for that Killing vector) by integrating over any two-surface containing the support of the gravitational field.

The concept of the momenta (linear and angular) of an *individual* hole in the presence of other holes cannot be rigorously defined in general relativity. However, a reasonable quasilocal definition for the momenta of an individual black hole is Eq. (A2) integrated over a two-surface exterior to that hole. For evaluating the components of the hole's linear momentum, we use the three translational Killing vectors of flat Euclidean three-space, and for the angular momentum, we use the three rotational Killing vectors with the origin of rotation chosen to be the center of the hole.

Following the conformal-imaging approach, the background extrinsic curvature of a spatial slice is constructed as the linear sum of "single-hole" extrinsic curvature solutions plus image terms that maintain an isometry condition (cf. Cook [7]). The background extrinsic curvature for a single black hole (including self-image terms) is parametrized directly in terms of the physical momenta measured at infinity. Evaluation of the black hole's momenta via the quasilocal definition is independent of the radius of the surface on which the integral is evaluated and always yields the correct physical result. Now consider evaluating the quasilocal momentum integral over a two-surface that does not contain the black hole. Using Gauss' law, we can rewrite the integral as

$$\Pi_{(k)} = \frac{1}{8\pi} \int \bar{\nabla}_j \left[\bar{\xi}^i_{(k)} \bar{A}^j_i \right] d^3\bar{V} = 0, \qquad \text{(A3)}$$

since $\bar{\xi}^i_{(k)}$ is a Killing vector of $\bar{\gamma}_{ij}$ and $\bar{A}^j_i$ satisfies the *vacuum* momentum constraint equation in this volume. Constructing a multihole extrinsic curvature from single-hole extrinsic curvature solutions, including self-image terms but not including general image terms, we see that Eq. (A3) implies that the contributions to the extrinsic curvature from additional holes do not affect the quasilocal momenta of a given hole.

What remains is to examine the contribution of general image terms to the quasilocal momenta of a hole. It seems reasonable that these terms should have no contribution, however, I have so far been unable to prove this analytically. Fortunately, it is straightforward to show numerically that general image terms make no contribution to the quasilocal momenta of either hole in a general binary configuration. More specifically, we can construct a general solution for the background extrinsic curvature, including any number of image terms. Computing the quasilocal momenta for either of the holes, we can use Richardson extrapolation to show that, up to the numerical precision of the computer, the results are *identical* to those obtained in the absence of any general image terms. This is independent of the sizes and separations of the holes and of the number of image terms included in the extrinsic curvature, implying that each image term *independently* contributes nothing to any of the surface integrals. I suspect that this result holds for any number of holes, however, this has not been verified.

We see then that within the limitations of defining the momenta of an individual hole, the momenta used to parametrize a single hole *are* the momenta of individual holes within a multihole configuration. That is, linear or angular momenta on one hole do not induce any amount of linear or angular momentum on any other hole in the system. In particular, the orbital angular momentum of a system of holes is well defined and does not contain an induced spin on any of the holes due to the linear momenta of the holes.

[1] G. B. Cook *et al.*, Phys. Rev. D **47**, 1471 (1993).
[2] J. W. York, Jr., in *Sources of Gravitational Radiation*, edited by L. L. Smarr (Cambridge University Press, Cambridge, England, 1979), pp. 83–126.
[3] J. M. Bowen, Gen. Relativ. Gravit. **11**, 227 (1979).
[4] J. M. Bowen and J. W. York, Jr., Phys. Rev. D **21**, 2047 (1980).
[5] J. M. Bowen, Gen. Relativ. Gravit. **14**, 1183 (1982).
[6] A. D. Kulkarni, L. C. Shepley, and J. W. York, Jr., Phys. Lett. **96A**, 228 (1983).
[7] G. B. Cook, Phys. Rev. D **44**, 2983 (1991).
[8] R. Arnowitt, S. Deser, and C. W. Misner, in *Gravitation: An Introduction to Current Research*, edited by L. Witten (Wiley, New York, 1962), pp. 227–265.
[9] J. K. Blackburn and S. Detweiler, Phys. Rev. D **46**, 2318 (1992).
[10] L. E. Kidder, C. M. Will, and A. G. Wiseman, Class. Quantum Gravit. **9**, L125 (1992).
[11] J. W. York, Jr., in *Frontiers in Numerical Relativity*, edited by C. R. Evans, L. S. Finn, and D. W. Hobill (Cambridge University Press, Cambridge, England, 1989), pp. 89–109.
[12] D. Christodoulou, Phys. Rev. Lett. **25**, 1596 (1970).
[13] G. B. Cook and J. W. York, Jr., Phys. Rev. D **41**, 1077 (1990).
[14] G. B. Cook and A. M. Abrahams, Phys. Rev. D **46**, 702 (1992).
[15] P. Anninos *et al.*, report, 1994 (unpublished).
[16] L. E. Kidder, C. M. Will, and A. G. Wiseman, Phys. Rev. D **47**, 3281 (1993).
[17] J. W. York, Jr., in *Essays in General Relativity*, edited by F. J. Tipler (Academic, New York, 1980), pp. 39–58.